Article

Current Biology

Bidirectional Propagation of Signals and Nutrients in Fungal Networks via Specialized Hyphae

Graphical Abstract

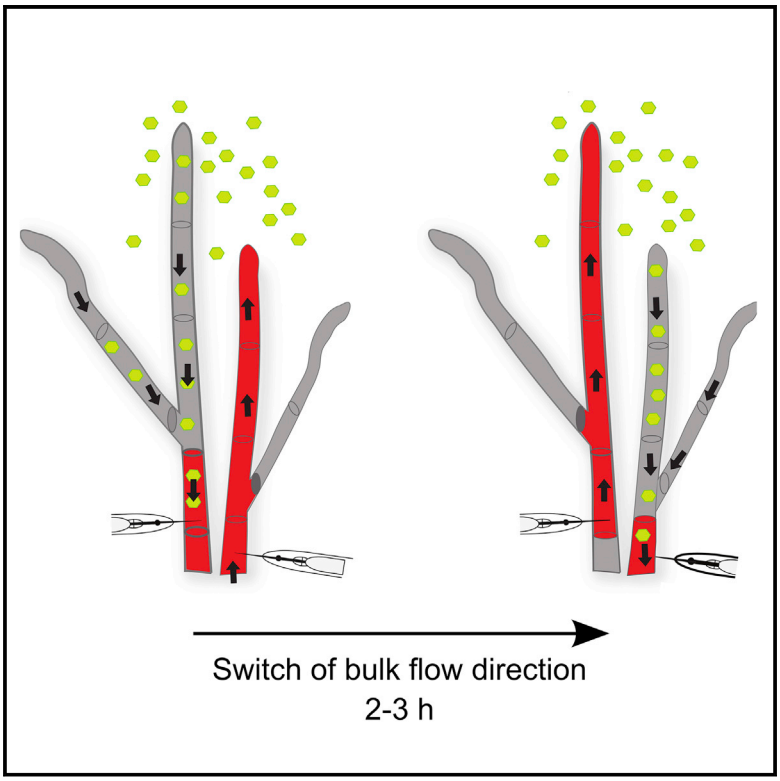

Authors

Stefanie S. Schmieder, Claire E. Stanley, Andrzej Rzepiela, ..., Andrew J. deMello, Markus Aebi, Markus Künzler

Correspondence

mkuenzle@ethz.ch

In Brief

Schmieder, Stanley et al. provide experimental evidence for the bidirectional propagation of signals and nutrients along specialized hyphae. These results, collected on a microfluidic chip, suggest that multicellular fungi use undescribed mechanisms to coordinate the distribution of nutrients and their behavioral response upon attack by fungivores.

Highlights

- Transport of signals and nutrients in fungal mycelia occurs via specialized hyphae
- Transport in these hyphae is bidirectional
- Direction of transport in these hyphae oscillates between acropetal and basipetal

Schmieder et al., 2019, Current Biology *29*, 217–228
January 21, 2019
https://doi.org/10.1016/j.cub.2018.11.058

CellPress

Current Biology
Article

Bidirectional Propagation of Signals and Nutrients in Fungal Networks via Specialized Hyphae

Stefanie S. Schmieder,[1,5,7] Claire E. Stanley,[2,6,7] Andrzej Rzepiela,[3] Dirk van Swaay,[2] Jerica Sabotič,[4] Simon F. Nørrelykke,[3] Andrew J. deMello,[2] Markus Aebi,[1] and Markus Künzler[1,8,*]
[1]Department of Biology, Institute of Microbiology, ETH Zürich, Zürich, Switzerland
[2]Department of Chemistry and Applied Biosciences, Institute for Chemical and Bioengineering, ETH Zürich, Zürich, Switzerland
[3]Scientific Center for Optical and Electron Microscopy, ETH Zürich, Switzerland
[4]Department of Biotechnology, Jožef Stefan Institute, Ljubljana, Slovenia
[5]Present address: Division of Gastroenterology, Boston Children's Hospital, Harvard Medical School, Boston, MA, USA
[6]Present address: Agroecology and Environment Research Division, Agroscope, Zürich, Switzerland
[7]These authors contributed equally
[8]Lead Contact
*Correspondence: mkuenzle@ethz.ch
https://doi.org/10.1016/j.cub.2018.11.058

SUMMARY

Intercellular distribution of nutrients and coordination of responses to internal and external cues via endogenous signaling molecules are hallmarks of multicellular organisms. Vegetative mycelia of multicellular fungi are syncytial networks of interconnected hyphae resulting from hyphal tip growth, branching, and fusion. Such mycelia can reach considerable dimensions and, thus, different parts can be exposed to quite different environmental conditions. Our knowledge about the mechanisms by which fungal mycelia can adjust nutrient gradients or coordinate their defense response to fungivores is scarce, in part due to limitations in technologies currently available for examining different parts of a mycelium over longer time periods at the microscopic level. Here, we combined a tailor-made microfluidic platform with time-lapse fluorescence microscopy to visualize the dynamic response of the vegetative mycelium of a basidiomycete to two different stimuli. The microfluidic platform allows simultaneous monitoring at both the colony and single-hypha level. We followed the dynamics of the distribution of a locally administered nutrient analog and the defense response to spatially confined predation by a fungivorous nematode. Although both responses of the mycelium were constrained locally, we observed long-distance propagation for both the nutrient analog and defense response in a subset of hyphae. This propagation along hyphae occurred in both acropetal and basipetal directions and, intriguingly, the direction was found to alternate every 3 hr in an individual hypha. These results suggest that multicellular fungi have, as of yet, undescribed mechanisms to coordinate the distribution of nutrients and their behavioral response upon attack by fungivores.

INTRODUCTION

Natural environments are heterogeneous in many aspects. Nutrient composition in the soil is subject to spatiotemporal variations, which create very distinct and ephemeral microhabitats [1]. Fungi cope with this discontinuous nutrient distribution by the formation of a continuous (syncytial) network of arrays of linearly arranged cells (hyphae), referred to as a mycelium, which allows them to access nutrient-rich microhabitats and to achieve nutritional homeostasis within all cells of the multicellular organism [2, 3].

Fungal mycelia grow by tip extension of individual hyphae, resulting in indeterminate radial growth, whereas secondary and further branches populate intermediary regions to optimize nutrient acquisition [4]. The formation of a network is accomplished by hyphal fusion (anastomosis) [5–7]. Depending on the fungal species, such networks can become quite large, ranging from cubic centimeters to many cubic meters, as is the case for ectomycorrhizal systems or cord-forming basidiomycetes [8]. The network as such can be continuously remodeled and is therefore highly dynamic, adapting to different underlying nutrient conditions, damage, or assault by meso-fauna [8–10]. Such network dynamics requires the reallocation of nutrients from different parts of the mycelium to allow, for example, bridging of nutrient-poor areas or damage repair [9–15]. Nutrient reallocation (in the form of radiotracers) through mycelial networks was predominantly examined and observed within cords or rhizomorphs of different basidiomycete species, where it is claimed to be important for the sufficient delivery and distribution of metabolically relevant nutrients to growing tips [16–19]. The driving force for this nutrient reallocation was hypothesized to be mainly pressure-driven mass flow [20–22]. However, the reported bidirectionality (acropetal and basipetal directions) of nutrient reallocation is difficult to explain with this model [20, 22–24]. Furthermore, the spatial scale at which mycelia operate in nature as a physically or physiologically integrated entity is not known [14].

Besides local fluctuations in physicochemical elements, biotic factors including microbial and faunal communities co-inhabiting a particular microhabitat give rise to considerable environmental

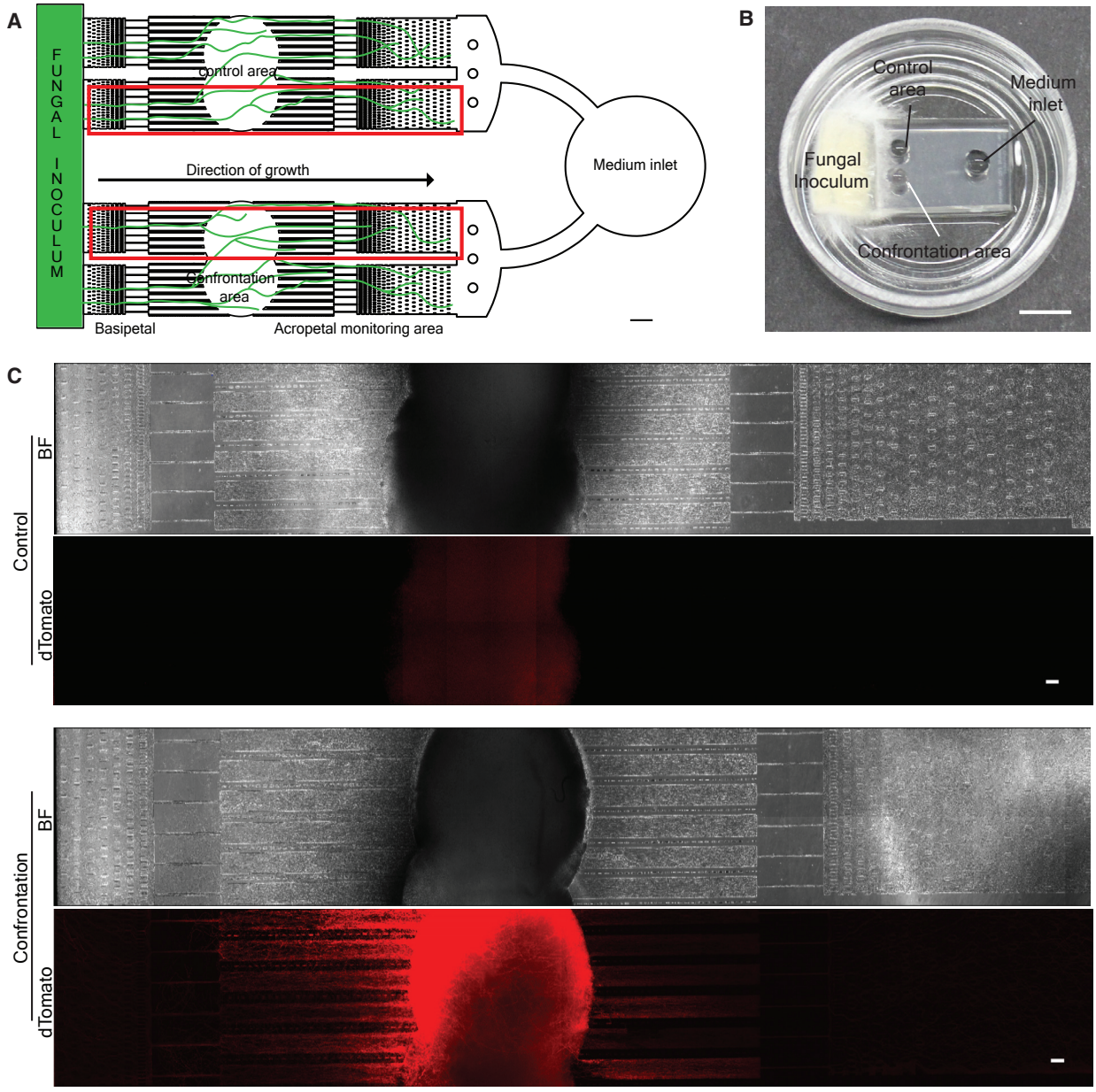

(legend on next page)

variations in space and time. For example, the sessile and heterotrophic lifestyle of fungi entails constraints when encountering competitors, predators, or parasites. In order to defend themselves against these antagonists, fungi have developed an impressive arsenal of toxic metabolites and proteins [25–29]. This defense response in fungi can be induced, as shown by the activation of secondary metabolite gene clusters [30–32]. The model mushroom *Coprinopsis cinerea* induces nematotoxic lectins upon challenge with the fungivorous nematode *Aphelenchus avenae* [33, 34]. Thus far, studies of inducible defense responses of fungal mycelia have focused on transcriptional and/or translational changes of the entire organism (mycelium). The defense response of individual hyphae, the eventual propagation of these local responses to other parts of the mycelium, as well as the ecological significance of such coordinated behavior remain to be elucidated [35–37].

In order to understand how the vegetative mycelium of *C. cinerea* responds to local changes in the environment, we developed a microfluidic platform designed to constrain the area of interaction between fungal mycelia and nematodes and visualize events occurring within individual hyphae (fungal-nematode-interaction [FNI] device). Microfluidic manipulation of fluid volumes on the microscale has been employed in a multitude of different biological disciplines, notably for the study of whole (living) organisms in recent years [38]. Importantly, our novel FNI platform enables the precise manipulation of the microenvironment, including the addition of nematodes and abiotic stimuli [39], and allows the fungus of interest, growing both within and outside of the confrontation area, to be monitored. In combination with high-resolution, automated imaging techniques, this platform facilitates the study of dynamic biological processes at the cellular level without losing spatial or temporal resolution. We constructed *C. cinerea* reporter strains to visualize and quantify the induction of genes coding for defense proteins upon challenge with nematodes. As a result of combining the reporter strain with the microfluidic platform, we were able to follow the defense response of the fungus in real time and with single-hypha resolution. The same setup was used to introduce the fluorescent glucose analog 2-Deoxy-2-[(7-nitro-2,1,3-benzoxadiazol-4-yl)amino]-D-glucose (2-NBDG) to precise locations within the microfluidic device to follow nutrient transport through the mycelium.

This experimental setup revealed that the transcriptional induction of *C. cinerea* defense genes in response to predation by *A. avenae* is mainly localized to those parts of the vegetative mycelium that are in direct contact with the predator. We could, however, identify a distinct hyphal subtype in the mycelium of this basidiomycete that was capable of propagating the defense response over several millimeters both in the acropetal and basipetal direction. Remarkably, our time-lapse studies revealed an oscillation of the fluorescence signal with a constant periodicity of approximately 4–6 hr within these hyphae. The same hyphal subtype also transported the glucose analog 2-NBDG with similar kinetics, but propagation of the defense signal and transport of 2-NBDG were mutually exclusive when triggered and applied, respectively, at opposite locations within the device. These findings can be explained by a periodical switch in the direction of solute transport and coordinated opening and closure of septa in these hyphae.

RESULTS

Local and Specific Defense Response of *C. cinerea* against the Fungivorous Nematode *A. avenae*

To monitor the spatial distribution of the *C. cinerea* defense response upon predation by *A. avenae* with cellular resolution, we first designed a microfluidic device (FNI) in which the access of nematodes to the growing mycelium is restricted to specific regions, namely the "confrontation area" (Figures 1A, 1B, S1A, and S1B). Spatial restriction is achieved by incorporating constriction channels between the confrontation area and the basipetal and acropetal monitoring areas. Due to their small width and height (10 μm) and long length (500 μm), nematodes cannot enter these channels. We also introduced a control area for examination of non-confronted hyphae of the same mycelial colony. Second, we constructed various *C. cinerea* AmBm reporter strains carrying either dTomato or eGFP expression cassettes driven by the promoters of the *cgl2* and *cctx2* genes to visualize the expression of these genes. The expression of both genes is induced in the vegetative mycelium of monokaryotic *C. cinerea* strain Okayama 7 under nematode feeding pressure, and the encoded proteins are toxic to different fungal foraging phyla [33, 34].

In our setup, induction of defense gene expression was most prominent for parts of the mycelium that were directly confronted

Figure 1. Local Induction of the *cgl2* Promoter in the *C. cinerea* Mycelium upon Nematode Predation

(A) Design of the fungal-nematode-interaction (FNI) microfluidic device. Scheme shows a two-dimensional overview of the microchannel geometry used to accommodate the fungal hyphae, originating from the inoculum, and inlets used for the application of nematodes (confrontation area with parallel control area) or solutes (medium inlet). The height of the microchannels within the entire device is 10 μm. Scale bar, 500 μm.

(B) Photograph of the FNI microfluidic device. In the example shown, the device was inoculated with *C. cinerea* on YMG agar and incubated for 18 hr at 37°C. Scale bar, 5 mm.

(C) Tiled bright-field and fluorescent image of the control and confrontation area of an FNI microfluidic device containing *C. cinerea* strain AmBm *cgl2p-dTom* 16 hr after co-inoculation with the fungivorous nematode *A. avenae*. Production of dTomato driven by the *cgl2* promoter was only visible in the confrontation, but not in the control area. Images represent the monitoring areas depicted by the red boxes in (A). Scale bars, 100 μm. BF, bright field.

(D) Quantification of dTomato production in the confrontation area over a 24 hr time course after co-inoculation of *A. avenae*. Relative fluorescence (mean gray values) of 1/4 of the confrontation and control area (24 hr ctrl) for six biological replicates is plotted. The 18 hr time point and 24 hr time point are statistically significantly different from the 24 hr control time point. A one-way ANOVA and Kruskal-Wallis test was performed. *$p < 0.05$, **$p < 0.01$. AU, arbitrary units. Error bars indicate SDs.

(E) qRT-PCR analysis of the nematode induction of the *cgl2* and *cctx2* genes in *C. cinerea* AmBm *cgl2p-dTom* using material extracted from the confrontation or control area in the FNI microfluidic device at two different time points after co-inoculation with *A. avenae*. Bars represent the mean $\log_2$ fold changes of the expression of the defense genes between confrontation and control areas among three replicates. Error bars indicate SDs.

See also Figure S1, Table S3, and Video S1.

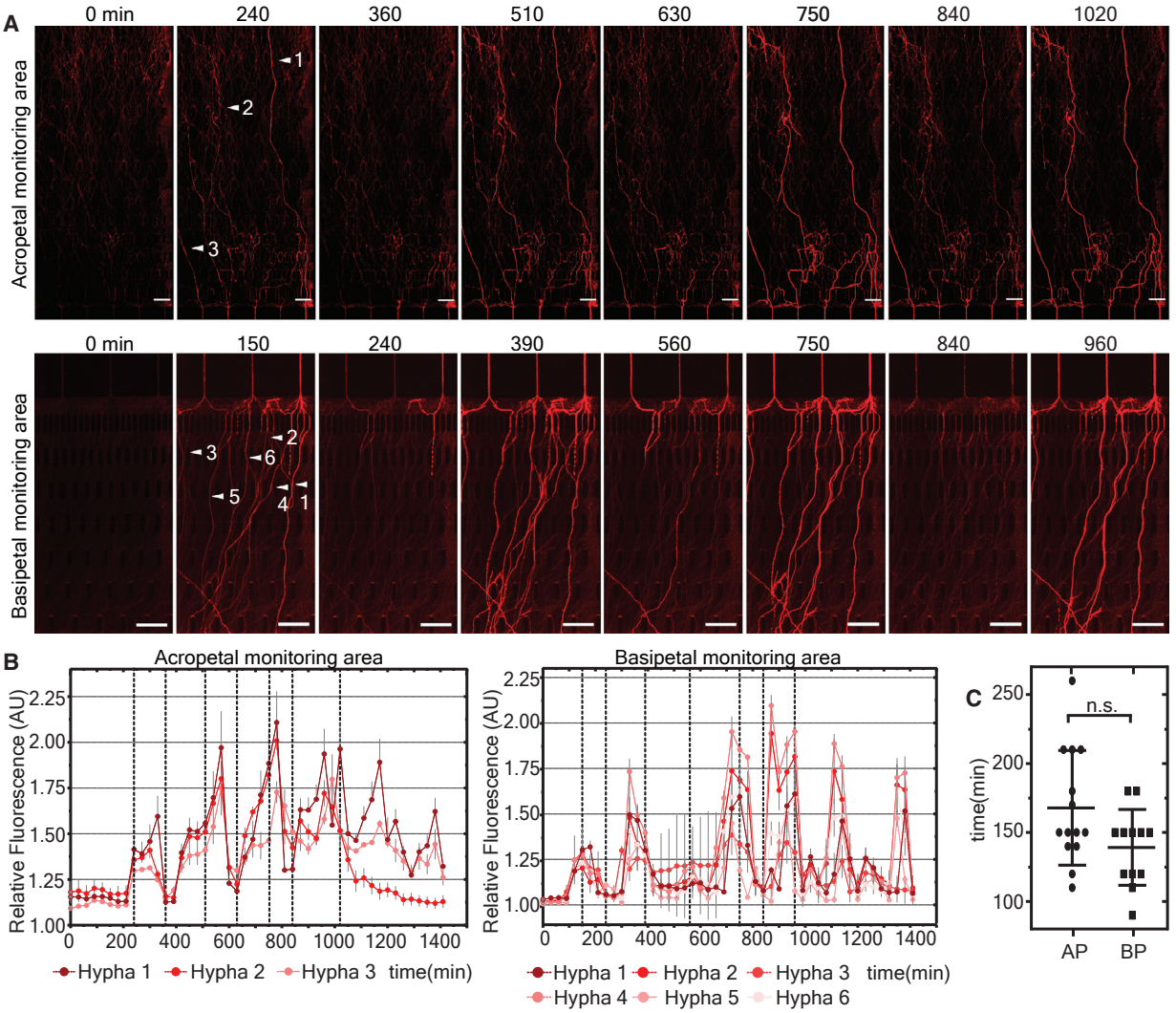

(legend on next page)

with the nematode (Figure 1C). Within the confrontation area, the vast majority of hyphae expressed dTomato at high levels, whereas in the control area, hyphae did not show any induction of the *cgl2p-dTom* reporter gene 18–24 hr after addition of the nematodes (Figures 1C and 1D).

The local induction of defense genes after nematode foraging was also demonstrated for the second reporter strain, *C. cinerea* AmBm *cctx2p-dTom*, encoding the dTomato expression cassette under the control of the promoter for the chimerolectin CCTX2. Again, production of dTomato was only detected when nematodes were present and not in the control area (Figure S1C). Because the level of dTomato production observed in this strain was lower, compared to dTomato production driven by the *cgl2* promoter, further analyses of the *C. cinerea* defense response were carried out with the *C. cinerea* AmBm *cgl2p-dTom* strain.

A. avenae feeds by piercing the hyphal cell wall and ingesting the content of a hyphal compartment (Video S1). The active feeding by *A. avenae* seems to be required for the induction of the *cgl2* promoter, because the application of dead *A. avenae* did not, in accordance with previous results [33], trigger dTomato production in *C. cinerea* AmBm *cgl2p-dTom* (Figure S1C). Induction of dTomato was also not detected when, instead of *A. avenae*, bacteria (*B. subtilis* 168 and *E. coli* Nissle 1917) were applied to the confrontation area (Figure S1C).

The production of nematotoxic lectins, as observed by the production of dTomato, was detectable as early as approximately 6 hr and became significant 18 hr after the addition of *A. avenae* to the confrontation area (Figures 1D and 1E). Thus, the expression of defense effector genes was detected significantly earlier using the microfluidic FNI device than described previously (48–72 hr after nematode inoculation) [34]. qRT-PCR analysis of *C. cinerea* AmBm *cgl2p-dTom* hyphae collected from the confrontation area 6 hr and 48 hr after nematode application confirmed the differential expression of *cgl2* and *cctx2* (Figure 1E).

Propagation of Defense Response in Trunk Hyphae

The above analysis of *C. cinerea* AmBm *cgl2p-dTom* challenged with *A. avenae* showed that the induction of the *C. cinerea* anti-nematode defense response was primarily localized within the confrontation area and did not propagate systemically throughout the entire mycelium (e.g., into the control area harboring hyphae of the same colony; Figure 1C). However, detailed analysis of the acropetal and basipetal monitoring areas, where hyphae do not come into direct contact with *A. avenae*, revealed a systemic propagation of the induction in a distinct subset of hyphae. This systemic induction within individual hyphae was observed acropetally, as well as basipetally, originating from the confrontation area (Figures 2A and 2B). dTomato fluorescence within such hyphae was observed to spread over long distances, in some instances over several millimeters (>2.5 mm). Importantly, the acropetal and basipetal transmission was not dependent on the promoter (*cgl2p*, *cctx2p*; data not shown) or the fluorescent protein used (dTomato, eGFP) (Figure S1D). The speed of propagation of the fluorescence signal in both directions was similar and determined to be approximately 5 μm/s. This value exceeds the apical growth rate of *C. cinerea* AmBm by a factor of about 75× (4.1 μm/min [39]). The dTomato fluorescence signal rarely spread from an induced hypha into secondary branches, but was found to propagate from one hypha to another via anastomosis bridges (Figures S2A and S2B). Interestingly, we could not detect any further propagation of the induction in the donor hyphae beyond the point of anastomosis.

Hyphae capable of long-distance propagation of the defense induction were otherwise not readily distinguishable from the rest of the hyphal population; however, the diameter of these hyphae appeared consistently large. We therefore analyzed the diameters of hyphae in the vegetative mycelium of *C. cinerea* AmBm. A two-step clustering analysis was performed and the results suggest that hyphae of a *C. cinerea* AmBm mycelium can be grouped into, on average, 2 or 3 distinct populations of hyphae based on the different hyphal diameters (Figures S2C and S2D). The average diameter of hyphae transmitting the dTomato fluorescence signal showed a mean diameter that clustered into the group of hyphae exhibiting a large diameter, here termed generally as trunk hyphae (Figure S2D) [13, 40].

Oscillation of Defense Response Propagation

We followed the dTomato fluorescence in trunk hyphae over time by acquiring a series of time-lapse images. The time-lapse series revealed that the fluorescence signal was propagated in the

Figure 2. Acropetal and Basipetal Propagation of *cgl2p-dTom* Induction in Specialized Hyphae

(A) *A. avenae* was introduced into the confrontation area of a microfluidic device containing the *C. cinerea* AmBm *cgl2p-dTom* reporter strain 16 hr prior to image acquisition. After this preincubation period, a time-lapse image series with a 30 min interval between frames was recorded. Arrowheads indicate the monitored hyphae and the location for the fluorescence intensity measurement. Representative images for acropetal and basipetal propagation are shown. Scale bars, 100 μm.

(B) Analysis of fluorescence mean gray values for hyphae in (A) over all time points for the acropetal and basipetal monitoring areas. Dashed lines indicate the time points represented in (A). Error bars indicate SDs.

(C) Comparison of the oscillation periods of dTomato propagation in the acropetal (AP) and basipetal (BP) direction. The periods were measured in at least eight independent experiments, with a maximum of two analyzed hyphae per experiment. A Mann-Whitney test was employed to assess statistical difference between AP and BP mean oscillation periods. Error bars indicate SDs. n.s., not significant.

(D) Propagation of the production of *cgl2p*-driven dTomH1 fusion protein. *A. avenae* was introduced into the confrontation area of a microfluidic device containing the *C. cinerea* AmBm *cgl2p-dTomH1* reporter strain 16 hr prior to monitoring the fluorescence intensity. Activation of *cgl2p* leads to the production of nuclearly localized dTomatoH1 fusion protein in the induced hyphae. Inset shows the extent of nuclear localization. Scale bars, 100 μm.

(E) Individually induced hyphae (indicated with arrowheads) can be observed in the acropetal and basipetal monitoring areas. Scale bars, 30 μm.

(F) Fluorescence profile over time for representative nuclei. Upper left: an overview of the basipetal monitoring area. Six nuclei in the basipetal monitoring area, indicated by the arrowheads, were chosen for the analysis. All six nuclei stem from different individual hyphae. Upper right: representative images taken from the time series of nucleus number 2. Scale bars, 100 μm and 10 μm, respectively. Lower: the change in fluorescence mean gray values of the six nuclei, shown in the overview, over time.

See also Figures S2 and S3, Table S3, and Video S2.

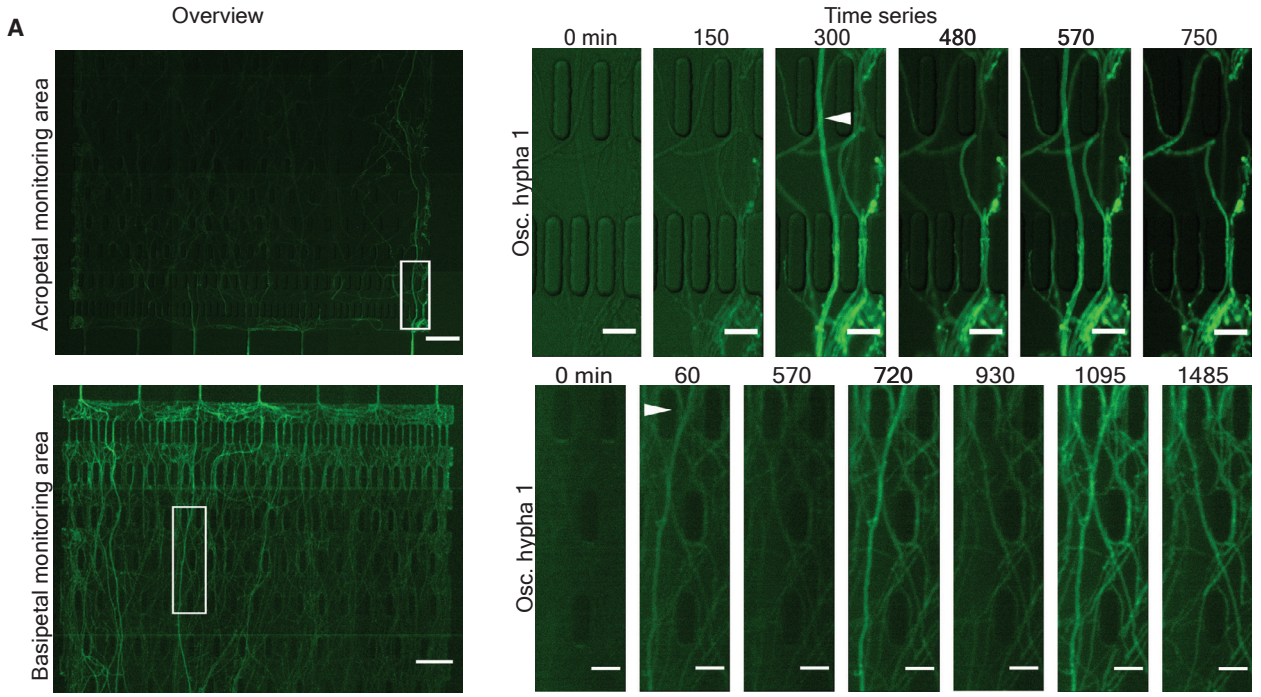

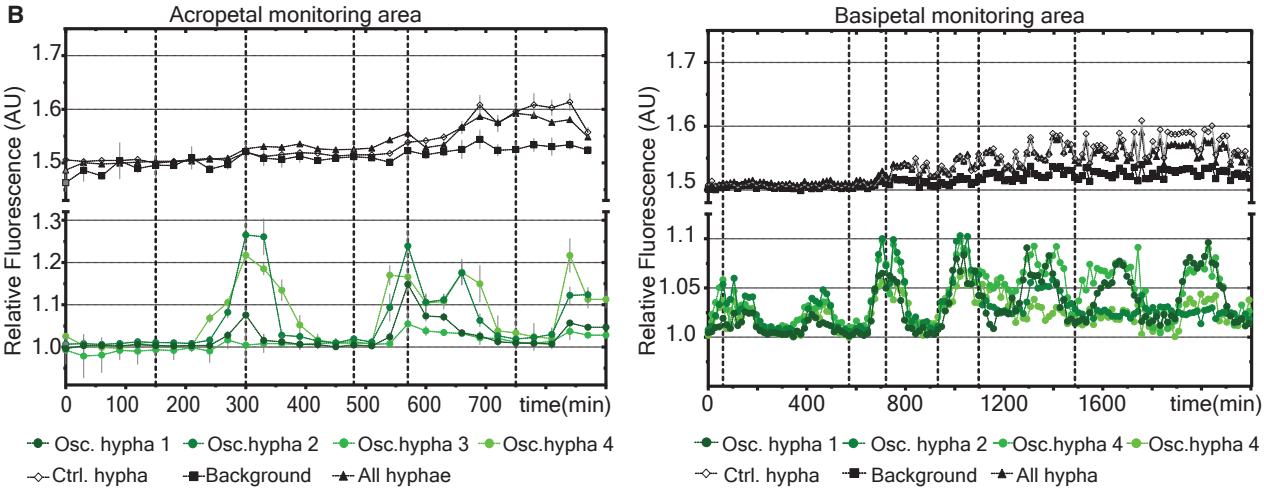

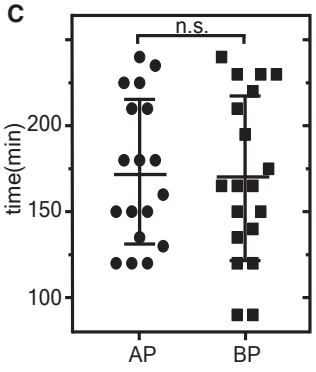

(legend on next page)

same hyphae several times within a 48 hr time frame, seemingly switching between an on/off state in a regular fashion (Figure 2A). We analyzed the fluorescence intensity profiles (mean gray values) of a section in several induced hyphae over time, and the analysis showed a periodicity of approximately 4–6 hr for the individual hyphae between induced and non-induced states in both directions (as illustrated in Figures 2B and 2C; Video S2).

The dTomato reporter protein was expressed as a cytosolic version that did not allow differentiation between diffusion/transport of the dTomato protein from its expression site, and/or the diffusion/transport of the underlying fungal defense inducer from the confrontation area. To determine whether the underlying fungal defense inducer is restricted to the site of nematode assault, we first constructed a *C. cinerea* AmBm reporter strain where dTomato localized to the nucleus. For this purpose, dTomato was fused to the *C. cinerea* histone H1 (*cgl2p-dTom*H1). When using this reporter strain, a fluorescence signal was observed in the nuclei of induced compartments and little to no dTomato was detected in the cytoplasm (Figures 2D and 2E). A detailed analysis of the co-cultivation between *A. avenae* and *C. cinerea* AmBm *cgl2p-dTom*H1 showed that the nuclear dTomato was still induced in distinct hyphae within the acropetal and basipetal monitoring areas, which were not directly in contact with the nematode (Figure 2E). However, unlike in *C. cinerea* AmBm *cgl2p-dTom*, which expresses the cytosolic version of dTomato, induced hyphae in *C. cinerea* AmBm *cgl2p-dTom*H1 did not show any "on/off" state (Figure 2F). The fluorescence signal in the nuclei in these hyphae remained stable or increased over the measuring period.

Second, we tested the opening states of the dolipore septa in the acropetally and basipetally induced trunk hyphae. For this purpose, we performed fluorescence bleaching experiments, because closed septa apparently represent a diffusion barrier for cytosolic dTomato in these hyphae (Figure S2A). The results indicate that, at the time of bleaching, not all septa along an induced hypha were open. The "−1 compartment" did not respond to the bleaching, indicating that the septa linking compartments 1 and −1 remained closed (Figures S3A–S3C). Furthermore, we observed that the opening state of a given septum can change over time. The septa connecting compartments 1 and −1 were closed at the time of the first bleaching, but opened 30 min later to allow transport of dTomato. The septa between compartments 3 and 4, on the other hand, closed during the time course (Figures S3D–S3F).

Transport of Nutrients in Trunk Hyphae

It is known that cord-forming basidiomycetes transport nutrients such as glucose or amino acids in a bidirectional manner and also show an oscillatory behavior [10, 20, 41]. Given the observed bidirectional propagation of the fungal defense response against nematodes within a specific subset of hyphae, we tested whether the same hyphae were also used for transport of solutes within the mycelium. For this purpose, we employed the soluble and fluorescent glucose analog 2-NBDG. Instead of applying *A. avenae*, 30 μM 2-NBDG was applied to the confrontation area and the fluorescence signal within the acropetal and basipetal monitoring areas was analyzed (Figure 3A). In contrast to the production of dTomato upon nematode challenge, distribution of 2-NBDG in the mycelium was far more complex. Septa of secondary or higher-order branches were permeable to 2-NBDG, leading ultimately to diffusion of 2-NBDG throughout the mycelium (Figure 3B, all hyphae). Furthermore, 2-NBDG diffusion within the chamber itself was observed (Figure 3B, background). Nonetheless, we could clearly detect a fluorescence signal in some distinct hyphae that exhibited a similar periodicity as those that had been induced by nematode challenge (Figure 3B, oscillatory hyphae). These hyphae showed transport of 2-NBDG both acropetally and basipetally, approximately 1 hr after application, whereas the arrival of 2-NBDG by general diffusion into the analyzed acropetal regions of interest (ROIs) was only apparent approximately 7–13 hr after application and did not show a periodicity (Figure 3B, control hypha, all hyphae).

When *A. avenae* and 2-NBDG were added to the confrontation area at the same time, the dTomato and 2-NBDG fluorescence signals propagated along the same trunk hyphae with a synchronous oscillation (Figures S4A–S4G). Given the strikingly similar behavior observed for both molecules, we analyzed the time required for one periodic event (Figures 2C and 3C) and found no statistical difference between dTomato and 2-NBDG or between acropetal and basipetal propagation (Figure S4H). To confirm a shared underlying distribution mechanism, we determined the theoretical concentration profile over time for dTomato (based on a 25-kDa model protein) and 2-NBDG (based on diffusion kinetics of a typical ion) assuming distribution by simple diffusion only, according to [24, 42] (Figures S5A and S5F).

The theoretical diffusion profile for dTomato is not in agreement with the fluorescence profile we obtained within propagating hyphae, suggesting that simple diffusion over large distances (>1,000 μm) alone cannot account for the fast dTomato

Figure 3. 2-NBDG Transport in the *C. cinerea* Mycelium

2-NBDG (30 μM) was added to the confrontation area and a time-lapse image series was acquired to track the distribution of 2-NBDG within the mycelium. A 15 min or 30 min time interval between frames was used for the acropetal and basipetal monitoring areas, respectively.

(A) Left: overview of an acropetal and basipetal monitoring area of two independent devices. Right: representative images taken from the time series of individual oscillating hyphae (indicated by arrowheads) for the insets marked in the respective overview. Scale bars, 100 μm (overview) and 20 μm (time series).

(B) Graph showing the mean gray values over time for four hyphae, where an oscillating 2-NBDG fluorescence signal was apparent (oscillating hyphae 1–4: green circles). The background fluorescence intensity in these regions increased over time without showing any periodicity (background: filled black square). This is also true for individual non-oscillating hyphae (control hypha: black open diamond), and for the total fluorescence intensity of all hyphae (all hyphae: black closed triangle). The dashed lines indicate the time points depicted in the time series. Error bars represent SDs.

(C) Comparison of the oscillation periods of 2-NBDG propagation in the acropetal (AP) and basipetal (BP) directions. The periods were measured in at least eight independent experiments, with a maximum of two hyphae per experiment. A Mann-Whitney test was performed to test for statistical significance. Error bars indicate SDs. n.s., not significant.

See also Figure S4 and Table S3.

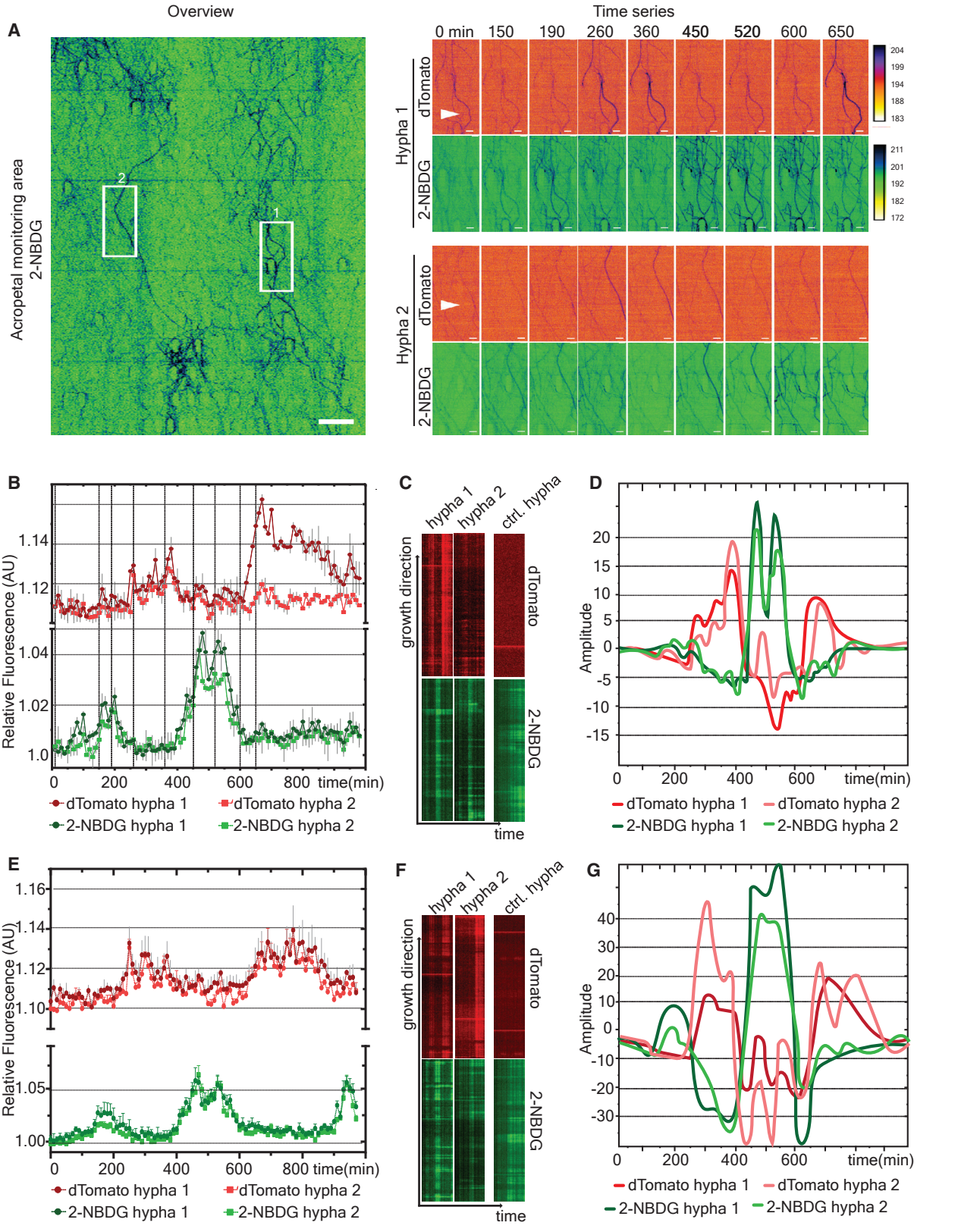

(legend on next page)

propagation kinetics observed (Figures S5B–S5E). Furthermore, the profile for 2-NBDG, although similar to the dTomato signal, also cannot be explained by a diffusion model, thus jointly suggesting a similar mechanism, different from diffusion, is underlying the transport of these two molecules.

Finally, we asked whether an individual trunk hypha mediates transport both in the acropetal and basipetal directions to potentially explain the on/off state. We therefore introduced *A. avenae* into the confrontation area and 2-NBDG into the medium inlet (see Figures S1A and S1B for the microfluidic device scheme). The results revealed that the defense response and 2-NBDG were still transported in the same hyphae, but that their transport was mutually exclusive and the oscillation of their transport was shifted by about half a period (2–3 hr) (Figures 4 and S4I).

DISCUSSION

The present study reveals a yet-undescribed functional differentiation of *C. cinerea* mycelia generating large trunk hyphae capable of bidirectional transport of bulk cytoplasmic solutes. This transport results in efficient distribution of nutrients and the systemic induction of defense genes, reaching a distance several millimeters from the actual site of predation.

Despite the broad versatility and variations in design, the application of microfluidic technology to study fungal growth and physiology or fungal interactions has only emerged in recent years [39, 43, 44]. The novel, tailor-made microfluidic device design presented here permitted the study of the dynamic interaction between the filamentous fungus *C. cinerea* and the fungivorous nematode *A. avenae* at the resolution of single hyphal compartments. In particular, the use of the FNI device to restrict the predatory nematode to specific mycelial areas, in combination with the use of fluorescent fungal reporter strains, made it possible to visualize the dynamic spatiotemporal distribution of the transcriptional response of the fungus to the nematode. It is anticipated that the setup and applications presented here, in particular the extraction of defined hyphal material, can be applied to many different physiological questions, where so far spatial resolution was lost due to the sampling technique employed.

The use of a fluorescent reporter strain in a microfluidic setup enabled us to follow the induction of defense genes of this fungus to nematode predation in real time and with single-cell resolution. Our results show that different parts of a basidiomycete mycelium are autonomous in their response to environmental stimuli, as the defense response was only elicited in areas directly confronted with the nematode (Figure 1C). Differences in gene expression and protein secretion between different hyphae of a mycelial colony were previously demonstrated for *Aspergillus niger* [45]. In contrast to *C. cinerea*, however, the observed gene expression differences within the *A. niger* mycelium were constitutive and not induced by external cues.

The strong response of the *C. cinerea* hyphae to *A. avenae* in the confrontation area of the microfluidic device allowed us to probe the specificity of this defense response (Figure S1C). Our observations confirmed previous results suggesting that inducible fungal defense is very specific for the respective antagonist and that the anti-nematode response relies on active feeding by the nematode [33, 34]. The time required to induce the anti-nematode response within the mycelium is comparable to the induction of plant defense against herbivory (Figures 1D and 1E) [46]. The fact that two different defense effector promotors (*cgl2p* and *cctx2p*) were activated with similar kinetics suggests that both promoters could be activated by the same signal-transduction pathway. The nature of the nematode signal perceived by the fungus, the mode of signal recognition, or the components of the signal-transduction pathways, however, remain to be elucidated.

In a subset of hyphae, characterized by their large diameter and referred to as trunk hyphae, the induction of the defense gene promotor was not limited to the site of predation but was propagated over several millimeters (Figure 2). Interestingly, this propagation occurred not only in the growth direction (acropetal) but also in the basipetal direction from the confrontation area (Figure 2A). The nuclearly targeted version of the dTomato reporter protein (*cgl2p-dTom*-H1) still showed

Figure 4. Bidirectional and Antiphase Propagation of *cgl2p-dTom* Induction and 2-NBDG within the Same Hypha

A. avenae was added to the confrontation area 24 hr prior to the addition of 30 μM 2-NBDG to the medium inlet of an FNI microfluidic device containing the *C. cinerea* AmBm *cgl2p-dTom* reporter strain. A time-lapse study was performed to determine whether acropetal and basipetal propagations of fluorescence occur simultaneously within the same hyphae.

(A) Left: overview of the 2-NBDG fluorescence intensity ca. 3 hr after addition of 2-NBDG to the medium inlet. Two regions of interest comprising exemplary propagating hyphae were selected and monitored for both dTomato and 2-NBDG fluorescence over time. The images were false colored using the inverted Green FIRE blue LUT (2-NBDG) and the inverted FIRE LUT (dTomato). Right: representative images taken from the time series of frames 1 and 2. Arrowheads indicate the hyphae monitored and the positions at which quantification in (B) was performed. Scale bars, 100 μm (overview) and 20 μm (time series).

(B) Graph showing the relative dTomato and 2-NBDG fluorescence intensities of the selected hyphae in the acropetal monitoring area over time. The dTomato fluorescence intensity values were shifted by 0.05 AU for visualization (see STAR Methods). The dashed lines indicate the time points shown in (A). Error bars represent SDs.

(C) Kymograph spanning the length of the two hyphae of interest in (A) and (B) and a control (non-oscillating) hypha; note the increase in 2-NBDG fluorescence over time for the control hypha, absent for the oscillating hyphae. Hyphae were traced in the growth direction over the whole field of view, and fluorescence intensity is plotted over time.

(D) Overlay of the oscillation behavior shown in (B) after spatial averaging and detrending. The signal-to-noise ratio of the time series was improved using spatial and temporal averaging with 7 × 7- and 5 × 5-pixel kernels, and the data were detrended with a rolling average of 30 prior to smoothing with a Hanning window.

(E) Graph as in (B) for two additional hyphae, of a different region of interest (ROI), showing the relative dTomato and 2-NBDG fluorescence intensities in the acropetal monitoring area over time. Error bars represent SDs.

(F) Kymograph as in (C) for the two hyphae of interest in (E) and a control (non-oscillating) hypha; note the increase in 2-NBDG fluorescence over time for the control hypha, absent for the oscillating hyphae.

(G) Overlay of the oscillation behavior shown in (E) after the spatial averaging and detrending performed as in (D).

See also Figures S4 and S5.

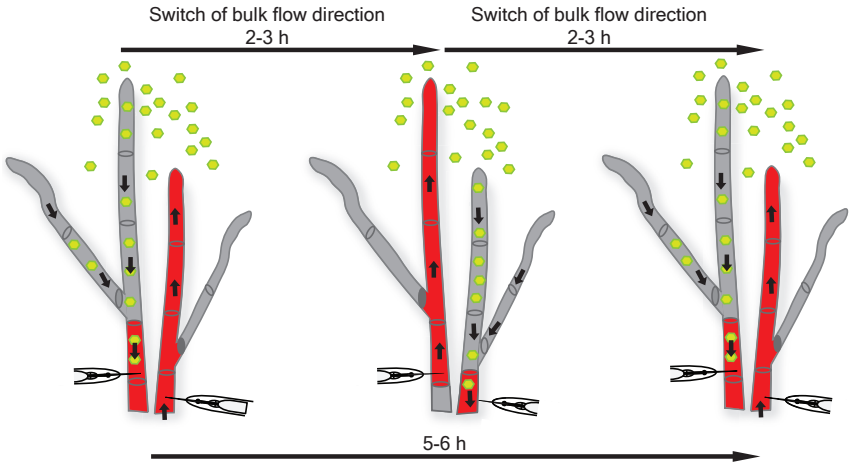

Figure 5. Model for Long-Distance Propagation of Gene Expression Patterns and the Distribution of Nutrients within Trunk Hyphae of *C. cinerea*

Based on the data presented in this study, we propose that a distinct subset of hyphae (trunk hyphae) in the *C. cinerea* AmutBmut mycelium possesses the ability to alternate the direction of their cytoplasmic bulk mass flow periodically (every 2–3 hr). In the basipetal flow mode, the septa along the trunk hyphae, including the ones toward the branches, are open to allow distribution of nutrients (2-NBDG) absorbed at the hyphal tips to subapical regions of the mycelium. Similarly, nematode assault leads to the induction of defense gene expression and the propagation of this expression pattern (most likely by bulk flow transport of an internal signal molecule) in the basipetal direction. In the acropetal flow mode, the septa along the trunk hyphae are open while the septa toward the branches are closed, channeling the propagation of signals and the distribution of nutrients in the (acropetal) direction of hyphal growth. The underlying molecular mechanisms that govern this behavior are unknown. Arrows indicate the direction of flow. Red filling represents induction of cytoplasmic dTomato expression in response to predation by nematodes (indicated by a schematic representation of their heads and stylets), whereas green hexagons within the hyphae represent nutrients (2-NBDG). See also Figures S3–S5.

acropetal and basipetal propagation along this subset of hyphae, indicating that, besides cytosolic dTomato, also the underlying inducer of the defense effector-encoding genes is transported. Because fluorescence of this nuclearly targeted version of dTomato did not, in contrast to the cytosolic dTomato, show any "on/off" state (Figures 2A and 2F), we hypothesize that oscillation of the cytosolic dTomato version is based on cytoplasmic flow.

The concept of acropetal and basipetal cytoplasmic flows within a fungal colony is not new. Previous studies demonstrated bidirectional nutrient translocation within cords or rhizomorphs of saprophytic and ectomycorrhizal basidiomycetes [8, 10, 20, 23, 41, 47, 48]. Bidirectionality was explained to be due to dedicated acro- and basipetally oriented hyphal bundles within cords or rhizomorphs. The use of periodic cytoplasmic flows to increase the dispersion of a molecule was also described for the network of syncytical veins in the slime mold *Physarum polycephalum* [48, 49]. Tlalka et al. showed for the first time that N transport (2-aminoisobutyric acid, [^{14}C]AIB) within cords of *Phaenerochate velutina* underlies a certain periodicity that was dependent on the subdomain of mycelium observed [50]. However, whereas transport of [^{14}C]AIB in *P. velutina* followed a pulsatile behavior with an oscillatory rhythm of around 11–14 hr [20, 50], the length of oscillation observed in our experiments was shorter (4–6 hr) and hyphal bundles or cords are not present in the vegetative mycelium of *C. cinerea* [51]. Instead, we could identify, using the novel microfluidic setup, a distinct subtype of individual hyphae, morphologically only distinguishable by their large diameter, that was responsible for the transport (Figures S2C and S2D).

In accordance with the cytoplasmic transport hypothesis for the observed phenomena with the fluorescent defense reporter strain, the application of a fluorescent glucose analog, 2-NBDG, used previously for the characterization of solute transport in hyphae of the ascomycete *A. niger* [52], to the *C. cinerea* mycelium, either independently or concomitantly with the nematode, revealed transport along the same hyphae with similar kinetics and periodicity as the dTomato fluorescence signal (Figures 3 and S4A–S4H). In addition, we find that neither the dTomato nor the 2-NBDG fluorescence signal propagation correlates with their respective expected diffusion kinetics (Figure S5).

Taken together, these results suggest the presence of a bulk transport of solutes within the *C. cinerea* mycelium, both in acropetal and basipetal directions, that covers distances beyond the dimensions of our microfluidic devices (3.5 mm) and may allow a fast and efficient distribution of nutrients and signals (Figures 5 and S5). In contrast to previous reports on other basidiomycetes, this bidirectional transport in *C. cinerea* appears to occur at the level of individual hyphae rather than bundles of hyphae (Figure 4). We speculate that the oscillation, observed for transport of both dTomato and 2-NBDG (Figures 2 and 3), is caused by periodical (every 2–3 hr) switching of the direction of bulk transport in these hyphae. Such a distribution mechanism of solutes would, on the one hand, equilibrate fluctuations and imbalances of individual nutrients between distant areas of the mycelium and ensure mycelial growth in environments where nutrients are distributed unevenly [12, 18, 48, 49]. On the other hand, the fast transmission of signals inducing anti-predator defense in areas of the mycelium that are not yet under attack might save vital parts of the mycelium from predator damage and thus ensure survival of the organism, as shown for plants [46]. This type of organismic defense is possible due to the ability of fungal mycelia to survive, even if large parts thereof are destroyed, and to regenerate from the remaining parts [35, 36].

At present, we can only speculate as to how the detected specialized transport hyphae in the vegetative mycelium of *C. cinerea* generate their cytoplasmic flow and periodically change its direction. Fluorescence bleaching and recovery experiments on induced hyphal compartments—outside of the confrontation area—indicate that the opening state of the septal pores in the propagating hyphae is reversible and that cytoplasmic continuity can be interrupted at a given time (Figure S3).

We hypothesize that the coordinated, reversible closure of the septal pores is a major factor in the bidirectional transport in these hyphae. The generation of such flows allows a faster and more efficient redistribution of nutrients and signals within the hyphal colony as compared to simple diffusion (Figures 3, 4, 5, S4, and S5) [24]. It remains to be elucidated as to why and how hyphal branches are connected and disconnected from this transport system.

In summary, the study of inducible defense against fungivorous nematodes in the basidiomycete *C. cinerea* has revealed a novel type of hyphal differentiation and communication within a fungal mycelium, and the next challenge will be to unravel the molecular mechanisms responsible for these phenomena.

STAR★METHODS

Detailed methods are provided in the online version of this paper and include the following:

- KEY RESOURCES TABLE
- CONTACT FOR REAGENT AND RESOURCE SHARING
- EXPERIMENTAL MODELS AND SUBJECT DETAILS
  - Strains and general cultivation conditions
- METHOD DETAILS
  - Generation of *C. cinerea* reporter strains
  - Microfluidic device design and manufacturing
  - Imaging of fungal-nematode co-cultures
- QUANTIFICATION AND STATISTICAL ANALYSIS
  - Validation of defense gene expression
  - Determination of hyphal diameter distribution
  - Fluorescence bleaching and generation of kymograph
  - Analysis of time-lapse image series
  - Phase mapping and cross-correlation analysis
  - Generation of diffusion model
  - Statistical analysis

SUPPLEMENTAL INFORMATION

Supplemental Information includes five figures, three tables, and two videos and can be found with this article online at https://doi.org/10.1016/j.cub.2018.11.058.

ACKNOWLEDGMENTS

Access to the Zeiss LSM780 was kindly provided by the Scientific Center for Optical and Electron Microscopy (ScopeM). This work was supported by the Swiss National Science Foundation (31003A_130671 to M.K. and PZ00P2_168005 to C.E.S.) and ETH Zürich.

AUTHOR CONTRIBUTIONS

Conceptualization, M.K.; Methodology, S.S.S., C.E.S., D.v.S., J.S., A.R., and S.F.N.; Investigation, S.S.S. and C.E.S.; Formal Analysis, S.S.S., C.E.S., A.R., and S.F.N.; Writing – Original Draft, S.S.S., C.E.S., and M.K.; Writing – Review & Editing, S.S.S., C.E.S., M.K., and A.R.; Visualization, S.S.S. and C.E.S.; Supervision, M.K., M.A., and A.J.dM.; Funding Acquisition, M.K.

DECLARATION OF INTERESTS

The authors declare no competing interests.

Received: July 4, 2018
Revised: October 5, 2018
Accepted: November 23, 2018
Published: January 3, 2019

REFERENCES

1. Hutchings, M., Wijesinghe, D., and John, E. (2000). The effects of heterogeneous nutrient supply on plant performance: a survey of responses, with special reference to clonal herbs. In The Ecological Consequences of Environmental Heterogeneity, M.J. Hutchings, E.A. John, and A.J.A. Stewart, eds. (Blackwell), pp. 91–110.
2. Burnett, J.H. (2003). Fungal Populations and Species (Oxford University Press).
3. Rayner, A., Griffith, G., and Ainsworth, A. (1995). Mycelial interconnectedness. In The Growing Fungus, N.A.R. Gow, and G.M. Gadd, eds. (Springer), pp. 21–40.
4. Prosser, J.I., and Trinci, A.P. (1979). A model for hyphal growth and branching. J. Gen. Microbiol. *111*, 153–164.
5. Glass, N.L., Rasmussen, C., Roca, M.G., and Read, N.D. (2004). Hyphal homing, fusion and mycelial interconnectedness. Trends Microbiol. *12*, 135–141.
6. Glass, N.L., Jacobson, D.J., and Shiu, P.K. (2000). The genetics of hyphal fusion and vegetative incompatibility in filamentous ascomycete fungi. Annu. Rev. Genet. *34*, 165–186.
7. Carlile, M.J., Watkinson, S.C., and Gooday, G.W. (2001). The Fungi, Second Edition (Academic Press).
8. Boddy, L. (1999). Saprotrophic cord-forming fungi: meeting the challenge of heterogeneous environments. Mycologia *91*, 13–32.
9. Fricker, M.D., Lee, J.A., Bebber, D.P., Tlalka, M., Hynes, J., Darrah, P.R., Watkinson, S.C., and Boddy, L. (2008). Imaging complex nutrient dynamics in mycelial networks. J. Microsc. *231*, 317–331.
10. Fricker, M.D., Tlalka, M., Bebber, D., Takagi, S., Watkinson, S.C., and Darrah, P.R. (2007). Fourier-based spatial mapping of oscillatory phenomena in fungi. Fungal Genet. Biol. *44*, 1077–1084.
11. Davidson, F.A., and Olsson, S. (2000). Translocation induced outgrowth of fungi in nutrient-free environments. J. Theor. Biol. *205*, 73–84.
12. Olsson, S. (2001). Colonial growth of fungi. In Biology of the Fungal Cell, Volume 8, R. Howard, and N.R. Gow, eds. (Springer), pp. 125–141.
13. Simonin, A., Palma-Guerrero, J., Fricker, M., and Glass, N.L. (2012). Physiological significance of network organization in fungi. Eukaryot. Cell *11*, 1345–1352.
14. Cairney, J.W. (2005). Basidiomycete mycelia in forest soils: dimensions, dynamics and roles in nutrient distribution. Mycol. Res. *109*, 7–20.
15. Bebber, D.P., Hynes, J., Darrah, P.R., Boddy, L., and Fricker, M.D. (2007). Biological solutions to transport network design. Proc. Biol. Sci. *274*, 2307–2315.
16. Agerer, R. (2001). Exploration types of ectomycorrhizae: a proposal to classify ectomycorrhizal mycelial systems according to their patterns of differentiation and putative ecological importance. Mycorrhiza *11*, 107–114.
17. Genney, D.R., Anderson, I.C., and Alexander, I.J. (2006). Fine-scale distribution of pine ectomycorrhizas and their extramatrical mycelium. New Phytol. *170*, 381–390.
18. Tlalka, M., Bebber, D., Darrah, P.R., and Watkinson, S.C. (2008). Mycelial networks: nutrient uptake, translocation and role in ecosystems. In British Mycological Society Symposia Series, Volume 28, L. Boddy, J.C. Frankland, and P. van West, eds. (Elsevier), pp. 43–62.
19. Watkinson, S.C., Boddy, L., Burton, K., Darrah, P.R., Eastwood, D., Fricker, M.D., and Tlalka, M. (2005). New approaches to investigating the function of mycelial networks. Mycologist *19*, 11–17.
20. Tlalka, M., Bebber, D.P., Darrah, P.R., Watkinson, S.C., and Fricker, M.D. (2008). Quantifying dynamic resource allocation illuminates foraging strategy in *Phanerochaete velutina*. Fungal Genet. Biol. *45*, 1111–1121.

21. Lew, R.R. (2011). How does a hypha grow? The biophysics of pressurized growth in fungi. Nat. Rev. Microbiol. *9*, 509–518.
22. Heaton, L., Obara, B., Grau, V., Jones, N., Nakagaki, T., Boddy, L., and Fricker, M.D. (2012). Analysis of fungal networks. Fungal Biol. Rev. *26*, 12–29.
23. Olsson, S., and Gray, S.N. (1998). Patterns and dynamics of ^{32}P-phosphate and labelled 2-aminoisobutyric acid (^{14}C-AIB) translocation in intact basidiomycete mycelia. FEMS Microbiol. Ecol. *26*, 109–120.
24. Fricker, M.D., Heaton, L.L.M., Jones, N.S., and Boddy, L. (2017). The mycelium as a network. Microbiol. Spectr. *5*, https://doi.org/10.1128/microbiolspec.FUNK-0033-2017.
25. Spiteller, P. (2008). Chemical defence strategies of higher fungi. Chemistry *14*, 9100–9110.
26. Rohlfs, M., and Churchill, A.C.L. (2011). Fungal secondary metabolites as modulators of interactions with insects and other arthropods. Fungal Genet. Biol. *48*, 23–34.
27. Stadler, M., and Sterner, O. (1998). Production of bioactive secondary metabolites in the fruit bodies of macrofungi as a response to injury. Phytochemistry *49*, 1013–1019.
28. Sabotič, J., Ohm, R.A., and Künzler, M. (2016). Entomotoxic and nematotoxic lectins and protease inhibitors from fungal fruiting bodies. Appl. Microbiol. Biotechnol. *100*, 91–111.
29. Wang, M., Triguéros, V., Paquereau, L., Chavant, L., and Fournier, D. (2002). Proteins as active compounds involved in insecticidal activity of mushroom fruitbodies. J. Econ. Entomol. *95*, 603–607.
30. Nützmann, H.-W., Reyes-Dominguez, Y., Scherlach, K., Schroeckh, V., Horn, F., Gacek, A., Schümann, J., Hertweck, C., Strauss, J., and Brakhage, A.A. (2011). Bacteria-induced natural product formation in the fungus *Aspergillus nidulans* requires Saga/Ada-mediated histone acetylation. Proc. Natl. Acad. Sci. USA *108*, 14282–14287.
31. Park, H.B., Kwon, H.C., Lee, C.-H., and Yang, H.O. (2009). Glionitrin A, an antibiotic-antitumor metabolite derived from competitive interaction between abandoned mine microbes. J. Nat. Prod. *72*, 248–252.
32. Brandt, P., García-Altares, M., Nett, M., Hertweck, C., and Hoffmeister, D. (2017). Induced chemical defense of a mushroom by a double-bond-shifting polyene synthase. Angew. Chem. Int. Ed. Engl. *56*, 5937–5941.
33. Bleuler-Martínez, S., Butschi, A., Garbani, M., Wälti, M.A., Wohlschlager, T., Potthoff, E., Sabotič, J., Pohleven, J., Lüthy, P., Hengartner, M.O., et al. (2011). A lectin-mediated resistance of higher fungi against predators and parasites. Mol. Ecol. *20*, 3056–3070.
34. Plaza, D.F., Schmieder, S.S., Lipzen, A., Lindquist, E., and Künzler, M. (2015). Identification of a novel nematotoxic protein by challenging the model mushroom *Coprinopsis cinerea* with a fungivorous nematode. G3 (Bethesda) *6*, 87–98.
35. Crowther, T.W., Boddy, L., and Hefin Jones, T. (2012). Functional and ecological consequences of saprotrophic fungus-grazer interactions. ISME J. *6*, 1992–2001.
36. Crowther, T.W., and A'Bear, A.D. (2012). Impacts of grazing soil fauna on decomposer fungi are species-specific and density-dependent. Fungal Ecol. *5*, 277–281.
37. Boddy, L., Wood, J., Redman, E., Hynes, J., and Fricker, M.D. (2010). Fungal network responses to grazing. Fungal Genet. Biol. *47*, 522–530.
38. Stanley, C.E., Grossmann, G., i Solvas, X.C., and deMello, A.J. (2016). Soil-on-a-chip: microfluidic platforms for environmental organismal studies. Lab Chip *16*, 228–241.
39. Stanley, C.E., Stöckli, M., van Swaay, D., Sabotič, J., Kallio, P.T., Künzler, M., deMello, A.J., and Aebi, M. (2014). Probing bacterial-fungal interactions at the single cell level. Integr. Biol. *6*, 935–945.
40. Bistis, G.N., Perkins, D.D., and Read, N.D. (2003). Different cell types in *Neurospora crassa*. Fungal Genet. Rep. *50*, 17–19.
41. Lindahl, B., Finlay, R., and Olsson, S. (2001). Simultaneous, bidirectional translocation of ^{32}P and ^{33}P between wood blocks connected by mycelial cords of *Hypholoma fasciculare*. New Phytol. *150*, 189–194.
42. Bokshtein, B.S., Mendelev, M.I., and Srolovitz, D.J., eds. (2005). Diffusion. In Thermodynamics and Kinetics in Materials Science: A Short Course (Oxford University Press), pp. 167–171.
43. Held, M., Edwards, C., and Nicolau, D.V. (2011). Probing the growth dynamics of *Neurospora crassa* with microfluidic structures. Fungal Biol. *115*, 493–505.
44. Hanson, K.L., Nicolau, D.V., Jr., Filipponi, L., Wang, L., Lee, A.P., and Nicolau, D.V. (2006). Fungi use efficient algorithms for the exploration of microfluidic networks. Small *2*, 1212–1220.
45. Vinck, A., de Bekker, C., Ossin, A., Ohm, R.A., de Vries, R.P., and Wösten, H.A.B. (2011). Heterogenic expression of genes encoding secreted proteins at the periphery of *Aspergillus niger* colonies. Environ. Microbiol. *13*, 216–225.
46. Toyota, M., Spencer, D., Sawai-Toyota, S., Jiaqi, W., Zhang, T., Koo, A.J., Howe, G.A., and Gilroy, S. (2018). Glutamate triggers long-distance, calcium-based plant defense signaling. Science *361*, 1112–1115.
47. Cairney, J.W.G. (1992). Translocation of solutes in ectomycorrhizal and saprotrophic rhizomorphs. Mycol. Res. *96*, 135–141.
48. Alim, K., Andrew, N., Pringle, A., and Brenner, M.P. (2017). Mechanism of signal propagation in *Physarum polycephalum*. Proc. Natl. Acad. Sci. USA *114*, 5136–5141.
49. Marbach, S., Alim, K., Andrew, N., Pringle, A., and Brenner, M.P. (2016). Pruning to increase Taylor dispersion in *Physarum polycephalum* networks. Phys. Rev. Lett. *117*, 178103.
50. Tlalka, M., Bebber, D.P., Darrah, P.R., Watkinson, S.C., and Fricker, M.D. (2007). Emergence of self-organised oscillatory domains in fungal mycelia. Fungal Genet. Biol. *44*, 1085–1095.
51. Kües, U. (2000). Life history and developmental processes in the basidiomycete *Coprinus cinereus*. Microbiol. Mol. Biol. Rev. *64*, 316–353.
52. Bleichrodt, R.J., Vinck, A., Read, N.D., and Wösten, H.A.B. (2015). Selective transport between heterogeneous hyphal compartments via the plasma membrane lining septal walls of *Aspergillus niger*. Fungal Genet. Biol. *82*, 193–200.
53. Schindelin, J., Arganda-Carreras, I., Frise, E., Kaynig, V., Longair, M., Pietzsch, T., Preibisch, S., Rueden, C., Saalfeld, S., Schmid, B., et al. (2012). Fiji: an open-source platform for biological-image analysis. Nat. Methods *9*, 676–682.
54. Staniland, L.N. (1954). A modification of the Baermann funnel technique for the collection of nematodes from plant material. J. Helminthol. *28*, 115–117.
55. Wälti, M.A., Villalba, C., Buser, R.M., Grünler, A., Aebi, M., and Künzler, M. (2006). Targeted gene silencing in the model mushroom *Coprinopsis cinerea* (*Coprinus cinereus*) by expression of homologous hairpin RNAs. Eukaryot. Cell *5*, 732–744.
56. Plaza, D.F., Lin, C.W., van der Velden, N.S., Aebi, M., and Künzler, M. (2014). Comparative transcriptomics of the model mushroom *Coprinopsis cinerea* reveals tissue-specific armories and a conserved circuitry for sexual development. BMC Genomics *15*, 492.

STAR★METHODS

KEY RESOURCES TABLE

REAGENT or RESOURCE	SOURCE	IDENTIFIER
Chemicals, Peptides, and Recombinant Proteins		
SU8 Photoresist	MicroChem	N/A
Sylgard 184 Kit	Biesterfeld Helvetia	Cat#5498840000
Ampicillin	Axon Lab	Cat#10020626
G418	BioConcept	Cat#4-15P01-GA
Nystatin	Sigma-Aldrich	Cat#N6261
Critical Commercial Assays		
PicoPure RNA Isolation Kit	Life Technologies, California, USA	Cat#KIT0204
Transcriptor Universal cDNA Master	Roche	Cat#05893151001
FastStart Unversal SYBR Green Master	Roche	Cat#04913850001
Experimental Models: Organisms/Strains		
See Table S1 for details regarding the strains used in this study	N/A	N/A
Growth Media (Composition / L)		
LB medium	10 g tryptone, 5 g yeast extract, 10 g NaCl	N/A
YMG medium	4 g glucose, 4 g yeast extract, 10 g malt extract	N/A
YPD medium	10 g yeast extract, 20 g peptone, 20 g dextrose	N/A
SD medium	6.7 g yeast nitrogen base, 20 g glucose, 5 g casamino acids, 20 mg tryptophan, 20 mg adenine sulfate, 20 mg tyrosine,	N/A
PDA medium	Fisher Scientific	Cat# DF0013-15-8
Oligonucleotides		
See Table S2 for details regarding the primer sequences used in this study	N/A	N/A
Recombinant DNA		
See Table S1 for details regarding plasmids used in this study	N/A	N/A
Restriction Enzymes		
*Bsr*GI	Thermo Scientific	Cat#ER0931
*Cla*I	Thermo Scientific	Cat#ER0141
*Xho*I	Thermo Scientific	Cat#ER0691
Software and Algorithms		
Fiji	[53]	https://fiji.sc/
Redox Ratio Analysis	[10]	https://markfricker.org/77-2/software/redox-ratio-analysis/redoxratio-analysis-software-download/
NIS-Elements Advanced Research	Nikon	N/A
Other		
Polyester Film Photolithography Mask	Micro Lithography Services Ltd. UK	Custom-made
100 mm Silicon Wafers	Silicon Materials	N/A
Hole Punch (cutting edge diameter: 3.02 mm)	Syneo	Cat#CR1341065N10R1
Hole Punch (cutting edge diameter: 2.49 mm)	Syneo	Cat#CR1090875N12R4
Hole Punch (cutting edge diameter: 1.65 mm)	Syneo	Cat#CR0720605N15R4
FluoroDish Cell Culture Dish	World Precision Instruments	Cat#FD35-100

CONTACT FOR REAGENT AND RESOURCE SHARING

Further information and requests for resources and reagents should be directed to and will be fulfilled by the Lead Contact, Markus Künzler (mkuenzle@ethz.ch).

EXPERIMENTAL MODELS AND SUBJECT DETAILS

Strains and general cultivation conditions

All organisms and strains used in this study are summarized in Table S1. Information on growth media and antibiotics can be found in the Key Resources Table. *Escherichia coli* DH5α was used for cloning and amplification of pRS426-derived plasmids and cultivated on Luria Bertani (LB) medium supplemented with 100 μg/mL ampicillin. *Escherichia coli* Nissle 1917 and *Bacillus subtilis* 168 were used to challenge the *Coprinopsis cinerea* reporter strains and both were grown in LB broth at 37°C [34]. *Saccharomyces cerevisiae* laboratory strain W303 (*MATa ade2-1 leu2-3,112 his3-11,15 ura3-1 can1-100 trp1-1*) was used for homologous recombination of plasmids and cultivated on YPD medium at 30°C as described [39]. Transformants were selected on SD medium without uracil.

Vegetative mycelium of *C. cinerea* strain A43mutB43mut (AmBm; homodikaryon) and the respective transformants were generally cultivated on YMG agar plates at 37°C in the dark. The fungivorous nematode *Aphelenchus avenae* (a kind gift from Prof. Richard Sikora, University of Bonn, Germany) was propagated at 20°C on vegetative mycelium of *Agaricus bisporus* pre-grown on PDA plates (Difco). Nematode harvesting was conducted using the Baermann funnel method [54]. In brief, a funnel was laid out with tissue paper to retain fungal and plate material and the bottom part was wrapped with aluminum foil. The fungal-nematode co-culture was then submerged into the water-filled funnel. After 12 hr the nematodes were collected by drawing the bottom 2 cm of water. After harvesting, nematodes were transferred to water agar plates supplemented with 200 μg/mL G418, 50 μg/mL Nystatin and 100 μg/mL Ampicillin, and incubated for 48 hr to eliminate all residual fungal contamination. *C. cinerea* AmBm - *A. avenae* co-cultivations were incubated at 20°C in the dark for the time indicated.

METHOD DETAILS

Generation of *C. cinerea* reporter strains

All plasmids used and generated in this study are listed in Table S1. All primer sequences can be found in Table S2. Plasmid pMA541, coding for a *cgl2p-dTomato* reporter gene in *C. cinerea,* was generated using pMA412, which encodes a dTomato expression cassette driven by the *A. bisporus gpdII* promoter and containing a *pab1* selection marker for *C. cinerea* in the vector backbone [39]. The *A. bisporus gpdII* promoter was replaced by the *C. cinerea cgl2* promoter (*cgl2p*). The *C. cinerea cgl2* promoter was amplified from genomic DNA with flanking homology regions for recombination into pMA412 (for primer sequences see Table S2). Homologous recombination of *Cla*I-*Xho*I opened pMA412 and the PCR-generated *cgl2p*-fragment was performed in *S. cerevisiae* W303. Selection of positive clones was done on SD medium without uracil [55]. Correct exchange of the *A. bisporus gpdII* promoter by the *C. cinerea cgl2* promoter resulting in plasmid pMA541 was confirmed by sequencing (Microsynth, Switzerland). Transformation of *C. cinerea* AmBm with pMA541 was carried out by protoplasting oidia as described previously [39, 55]. Nuclear localization of dTomato was achieved by fusing the coding region for dTomato to the one for histone H1 from *C. cinerea* (JGI Protein ID 467558) to create a H1-dTomato fusion protein. The plasmid pMA1130 was generated by amplifying the complete 467558 coding region (including introns) from genomic DNA with corresponding flanking homology regions for homologous integration into pMA541. pMA541 was linearized using the restriction enzyme *Fsp*AI (Thermo Scientific, California, USA).

Plasmid pMA1101 was generated in the same manner as pMA541 but amplifying the *cctx2* promoter region with corresponding flanking regions for recombination into pMA412 [34]. For pMA1131, the dTomato expression cassette in pMA541 was exchanged for an eGFP cassette with the intron-exon structure of the *cgl2* locus. Latter cassette was amplified from plasmid 341 (pRS426-benA-cgl2::eGFP) [55] with the respective flanking homology regions for integration into pMA541. Plasmid pMA541 was linearized using *Bsr*GI for this purpose. Homologous recombination as well as transformation into *C. cinerea* AmBm was performed as described above.

Microfluidic device design and manufacturing

Microfluidic devices were prepared as described in Stanley et al. [39]. In brief: Master molds were manufactured using a polyester film photolithography mask (Micro Lithography Services Ltd. UK) and a 100 mm silicon wafer (Silicon Materials, Germany) spin-coated with SU-8 photoresist (MicroChem, USA) aiming for a target height of 10 μm. Poly(dimethylsiloxane) (PDMS) silicone elastomer was prepared using a 10:1 ratio of base to curing agent (Sylgard 184, Dow Corning, USA) that was thoroughly mixed, degassed and then poured onto the master mold. After curing overnight at 70°C, the PDMS was removed from the mold and diced into slabs. A precision cutter (Syneo, USA), having a cutting edge diameter of 3.02 mm, was used to punch the holes for the medium inlet. The control and confrontation areas were always kept consistent between experiments, each corresponding to an area of ca. 5 mm^2 (Figures 1A, 1B, S1A, and S1B). Precision cutters with a cutting edge diameter of 1.65 or 2.49 mm were used to create the control/confrontation areas.

PDMS slabs and glass-bottomed Petri dishes (World Precision Instruments) were washed in 0.5 M sodium hydroxide (Sigma-Aldrich, Germany), 70% v/v ethanol, and sterile double distilled water (ddH2O). The PDMS slabs and Petri dishes were then dried at 70°C for 1 hr, bonded and filled with sterile-filtered yeast maltose glucose (YMG) medium.

Imaging of fungal-nematode co-cultures

The respective *C. cinerea* strain was cultivated at 37°C in a dark, humid box for 72 hr. Inoculation of a YMG-filled microfluidic device was performed as described in Stanley et al. [39] with the following modification: the inoculated microfluidic device was incubated in the dark with high humidity for approximately 18 hr at 37°C to allow the hyphae to grow into the confrontation and control areas (Figures 1A, 1B, S1A, and S1B) before the addition of nematodes. For every experiment, approx. 5 nematodes of a mixed stage population were transferred into the inlet that leads to the confrontation area. Following the addition of nematodes, the co-cultivation devices were monitored immediately or transferred to 20°C in the dark for later use.

Image acquisition was performed as described in Stanley et al. [39]. In brief, a Nikon Ti-U inverted widefield fluorescence microscope, was used for long-term, time-lapse experiments. The microscope was equipped with a Prior ProScan III motorized stage (Prior Scientific, UK) and a CoolSNAP HQ2 camera (Photometrics, Germany). Bright field images were acquired with using phase contrast microscopy with a × 20/0.45 NA S Plan Fluor objective lens (Nikon, Switzerland), and 100 ms exposure time.

Epifluorescence images were captured using a Nikon Intensilight C-HGFI mercury lamp (Nikon, Switzerland) as the source of excitation. TRITC and FITC HC BrightLine Basic Filtersets (AHF Analysentechnik, Germany) were used to image dTomato expression and the fluorescent glucose analog 2-NBDG (Life technologies) respectively (with exposure times of 100 and 200 ms respectively). Imaging experiments were coordinated with NIS-Elements Advanced Research imaging software (Nikon, Switzerland) and performed in a temperature controlled dark room at 20°C.

Images were analyzed using open software Fiji [53]. To measure the hyphal diameter the free hand tool and measuring tool of Fiji were used. The measuring tool was also used to analyze gray values.

QUANTIFICATION AND STATISTICAL ANALYSIS

Validation of defense gene expression

To validate the expression levels of the nematotoxin-encoding *C. cinerea* genes *cgl2* and *cctx2*, hyphal material was extracted from the confrontation area after 6 and 48 hr and flash frozen in liquid nitrogen. Hyphae were lysed using glass beads, as described previously [34, 56]. Total RNA was extracted using a PicoPure RNA isolation kit (Life Technologies, California, USA). The quality of the extracted RNA was controlled using a Bioanalyzer 2100 (Agilent). Quantitative real-time polymerase chain reaction (qRT-PCR) for the individual defense genes was carried out according to Plaza et al. [34]. In brief, single-stranded cDNA was synthesized using Transcriptor Universal cDNA Master (Roche). qRT-PCR reactions (20 μL) were prepared by adding 900 nM of the respective primer pair, 10 μL 2x FastStart Universal SYBR Green Master (Roche) and 10 ng cDNA template. The following qRT-PCR program was used: a hold step at 95°C for 15 min followed by 40 cycles of 95°C for 15 s, 62°C for 30 s and 72°C for 30 s. Primer sequences are described in Table S2.

Amplification cycles and PCR efficiencies were determined using LinRegPCR 12 program (BioGazelle). Differential expression ratios were calculated using the Ct difference formula [34].

Determination of hyphal diameter distribution

C. cinerea AmBm *cgl2p-dTom* was grown into a microfluidic device as described above, but incubation at 37°C was prolonged to 72 hr so that the fungus had completely covered the acropetal monitoring area. Bright-field images were acquired in the acropetal monitoring area and around 250 hyphal diameters were measured by hand using the straight line tool in Fiji (ImageJ software). Data from two independent experiments were pooled. For the diameter of transporting hyphae, data of several independent experiments (defense-induced hyphae as well as 2-NBDG transporting hyphae) were pooled. Normal distribution of hyphal diameters was tested using the Shapiro-Wilk's test with a 95% confidence interval in GraphPad Prism (GraphPad Software, USA). None of the experiments passed the normality test. 2-Step clustering analysis was performed using SPSS Statistics Software (IBM). One-way ANOVA with Bonferroni correction was performed to test if one of the three hyphal subpopulations and hyphae, capable of long distance transport, were statistically similar.

Fluorescence bleaching and generation of kymograph

A. avenae was added into the confrontation area of a microfluidic device containing the *C. cinerea* AmBm *cgl2p-dTom* reporter strain for 24 hr to induce dTomato expression. A propagating hypha in the acropetal monitoring area was chosen for bleaching. Bleaching was performed on a Zeiss LSM780 confocal microscope with 100 iterations using the maximum laser intensity either once or repeatedly every 20 s and images were acquired every 2 s thereafter. The Fiji segmented-line tool was used to trace the induced hypha throughout the imaging frame. To generate a fluorescence profile of the bleached hypha over time (kymograph), the Fiji Reslice tool was used. The kymograph displays the change in fluorescence intensity along the bleached hypha as a function of time. The gray values of the traced hyphae were exported for the indicated time points and blotted over the length of the hypha to determine responsive compartments.

Analysis of time-lapse image series

Absolute fluorescence intensities were measured at each time point within a time-lapse image series. To acquire a measurement, the Fiji tool "rectangular" was used to create a square ROI, which was placed exactly on the hypha of interest (covering the complete diameter of the hypha). To measure the relative fluorescence intensity, the background fluorescence intensity was estimated by

placing the same square ROI next to the hypha. The value of the absolute fluorescence intensity within the hypha was then divided by the background fluorescence intensity. This was repeated three times to yield an average value for one hypha. Values in arbitrary units (AU) were subsequently plotted as a function of time.

For 2-NBDG transport, fluorescence intensity measurements were performed additionally for all hyphae within an ROI covering most of the acropetal or basipetal monitoring area. To this end, the fluorescent image was thresholded and a mask created for all hyphae within the ROI. The fluorescence intensity was measured for all hyphae within the mask, summed and plotted against time. In Figure 3 and 0.5 AUs were added to simplify visualization within the graphs for the individual control hyphae, as well as for the background and the ROIs. Similarly in Figures 4 and S4, 0.05 AU and 0.5 AU were added for the dTomato fluorescence datasets to aid visualization. Experiments were excluded due to the following: no transport into acropetal or basipetal monitoring area visible, background fluorescence too high, induction of dTomato expression/intra-hyphal NBDG signal too low.

Phase mapping and cross-correlation analysis

The data manipulation was performed using a free MATLAB package available at https://markfricker.org/77-2/software/redox-ratio-analysis/redox-ratio-analysis-software-download/ (access July, 2016) [10] and the MapleSoft software package CrossCorrelation for cross-correlation analysis. The signal-to-noise ratio of the time series was improved using spatial and temporal averaging with 7x7 and 5x5 pixel kernel for each pixel and detrended with rolling average of 30, additionally a Hanning window was applied prior to a Discrete Fourier transform with a padding of 128 to extract better phase profiles for dTomato and 2-NBDG.

Fluorescent intensity values of hyphae 1 and 2 and hypha 1 plotted in Figures 4B and 4E, respectively, were used for cross-correlation analysis between dTomato and 2-NBDG signals.

Generation of diffusion model

The one dimensional, one directional diffusion was modeled using analytical solution from [2] (Equation 2.26). This model allows one to study how the concentration of a substance, characterized by a given diffusion constant D, evolves in time when it diffuses from a source, with a constant concentration $c = 1$ (arbitrary units), inside e.g., linear hyphae (one dimensional, open system with concentration c of a substance equal 0 at time $t = 0$ (s)). The model (Figure S5) was solved for several positions starting at 300 μm from the source bath for two substances characterized by D_1 and D_2 (which corresponds to a diffusion of a protein and an ion, respectively in a hypha [1]).

To determine the flow kinetics for dTomato and 2-NBDG in propagating hyphae, mean gray values were determined for two different points along the hypha (distance between the points is indicated in the graph). The hyphae were each chosen from two representative time-lapse experiments (Figures 2 and S4A for dTomato and Figure 3 for 2-NBDG).

Statistical analysis

SPSS Statistics Software (IBM) was used for 2-step clustering analysis and MATLAB software (MathWorks, USA) was used for cross-correlation analysis. For all other statistical analyses, GraphPad Software, USA was used. Details regarding all statistical analyses performed and software used can be found in the Table S3, the main text and the respective figure legends.